(Received 13 April 2024, Accepted 11 June 2024, Scheduled 20 June 2024)

A Miniaturized Lens Unit Based on Current Path Extension as a Wireless Power Transfer Medium at 2.45 GHz

Xingyue Liu, Zhiwei Liu*, Cheng Qiu, Zehua Luo, and Yuxin Deng

Department of Communication Engineering, East China Jiaotong University, Nanchang 330013, China

ABSTRACT: A novel miniaturized lens unit at 2.45 GHz is presented in this manuscript. This unit is formed by a modified Malta cross and an ordinary cross, with a unit period of $0.2\lambda_0$, where λ_0 denotes the unit wavelength. The ordinary cross unit creates a pathway for the current between two units. Accordingly, it increases the current path and reduces the unit volume to a quarter of its original size. By adjusting the length of the Malta cross arm, it is possible to achieve the transmission phase at 2.45 GHz within a range of 0–360°. Moreover, an improved PSO algorithm is used to optimize the phase of array elements. The optimization process is able to achieve a phase-shifting of $\pm 18°$ within the range of $3.28\lambda_0$. Simulation and measurement results show that the miniaturized lens unit can be used in the wireless energy transmission system.

1. INTRODUCTION

Based on transmission distance and frequency range, wireless energy transfer (WPT) can be divided into different categories including capacitive power transfer [1], magnetically coupled resonance wireless power transfer [2], inductive coupled wireless power transfer [3], microwave power transfer [4], and laser power transfer [5]. Compared with other WPT categories, microwave power transfer has significant advantages in terms of efficiency, flexibility, and safety due to the propagation characteristics of microwave [6]. Obviously, high-gain antennas play a crucial role in the field of microwave WPT [7]. Its high efficiency supports the stability and reliability of long-distance transmission. In addition, directivity improvement of the antenna can reduce energy scattering and loss during transmission, causing significant improvement of transmission efficiency. Therefore, high-gain antennas have significant advantages in the field of wireless energy transmission, improving transmission efficiency, stability, and security. Theoretically, high gain antennas can be realized using lens antennas [8]. Compared to regular optical lenses, using lens based on left-handed materials to form the properties of wide bandwidth, flexible manufacturing, miniaturization, and multifunctionality is a suitable way to meet the practical application. In 1968, Veselago discovered the backward wave property of left-handed medium [9]. In 2003, Cubukcu et al. found that left-handed materials have the ability to focus electromagnetic waves [10]. From 2005 to 2006, Antoniades and Eleftheriades [11] and Bonache et al. [12] verified the negative refraction and super-focusing phenomena of monochromatic waves in photonic crystals. These achievements have provided a solid theoretical foundation for the application of left-handed materials in the field of microwave lens.

Due to uneven unit distribution, oversized dimensions of the left-hand material unit can lead to various problems such as decreased anisotropy and refractive index [13]. The usual methods for achieving unit miniaturization are divided into three categories including designing a curved branch structure based on transmission line theory, using a lens unit with two different structures complemented with each other, and adding lumped elements on the unit to achieve miniaturization [14]. Ma et al. proposed a 7-layer lens structure, which uses metal patches and etched grooves overlapping each other, with a unit period of only $0.15\lambda_0$ [15]. The fractal design reduces the size of the lens unit by increasing the equivalent electrical length through the use of space filling. The complementation of the etching groove and metal antenna is used to miniaturize the lens unit further and expand frequency bandwidth. Sun et al. proposed a 6-layer transmission array structure with double-sided printing containing capacitors and varactor diodes, with a unit period of only $0.07\lambda_0$ [16]. The 6-layer lens structure is placed in front of the feeding array as a radome, and the varactor diodes´capacitance is changed by controlling the DC voltage with a computer to achieve beam scan. These methods are difficult to realize covering a 360° transmission phase range. A common solution to solve this kind of problem is to increase the number of layers of the lens [17].

In this article, a novel miniaturized structure is proposed, which consists of a modified Malta cross structure and a regular cross structure, with a unit period of $0.2\lambda_0$. By changing the arm length of the Malta cross, full 360° transmission phase at 2.45 GHz can be achieved through a 4-layer structure. The results of experiments and tests are proposed and discussed.

* Corresponding author: Zhiwei Liu (zwliu1982@hotmail.com).

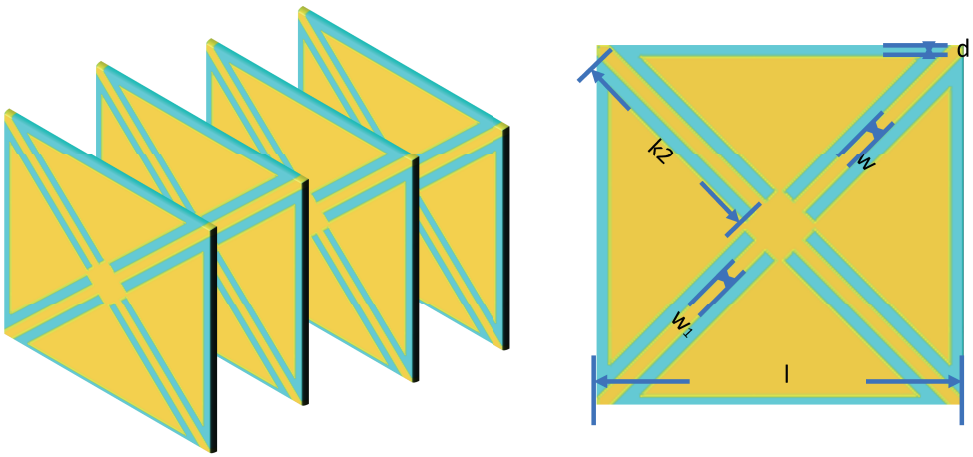

FIGURE 1. Matar cross unit structure and dimensions.

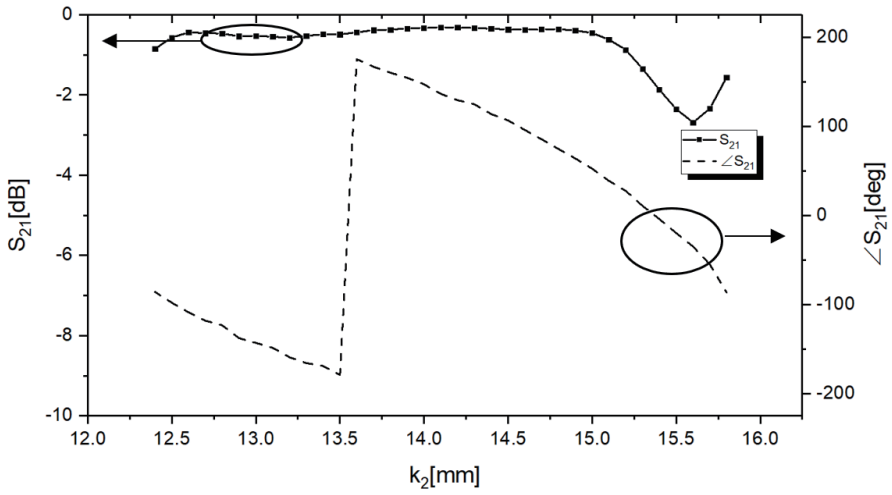

FIGURE 2. S parameter of simulation results with k_2.

2. STRUCTURE DESCRIPTION OF THE CONCEPTUAL MODEL

As shown in Figure 1, the miniaturized lens unit with a unit period of $0.2\lambda_0$ is shown. The metallic patterns are printed on four F4b substrates ($\varepsilon_r = 2.65$, $\tan\sigma = 0.015$). The spacing between two layers is 25 mm. The dimensions of the unit are shown in Table 1. The number of layers directly affects the number of resonance points, operating bandwidth, and the range of transmission phase.

TABLE 1. The value of parameter.

Parameter	d	w	w_1	l
Value (mm)	0.8	1	1	25

The miniaturized units with different lengths of arms are simulated using CST Microwave Studio software. The variation of transmission amplitude $|S_{21}|$ and transmission phase $\angle S_{21}$ with k_2 at 2.45 GHz is shown in Figure 2. From the figure, it can be seen that the transmission phase $\angle S_{21}$ achieves a complete 360° phase coverage, with the transmission amplitude $|S_{21}|$ less than -3 dB.

3. OPERATION PRINCIPLE

The S_{11} results of the Malta cross structure and miniaturized structure are shown in Figure 3 and Figure 4. In Figure 4, the S_{11} result of the miniaturized unit is presented. Compared to the Malta structure, adding a cross structure can introduce a new resonance point at low frequencies.

As shown in Figure 5, the current distribution of a single-layer Malta cross unit at 2.45 GHz is given. It can be seen that the current distribution between two arms of the Malta cross is stronger, and the current path is approximately twice the length of the Malta cross arm. The single-layer Malta cross electric field distribution is shown in Figure 6. When electromagnetic waves pass through a gap, they will form a closely coupled region of electric and magnetic fields near the gap, thereby generating current.

The current distribution diagram of a single-layer miniaturized unit at 2.45 GHz is given in Figure 7. It can be seen that

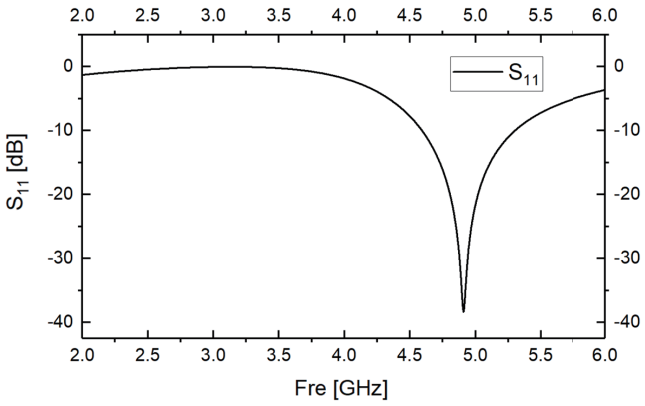

FIGURE 3. S_{11} of Malta cross structure.

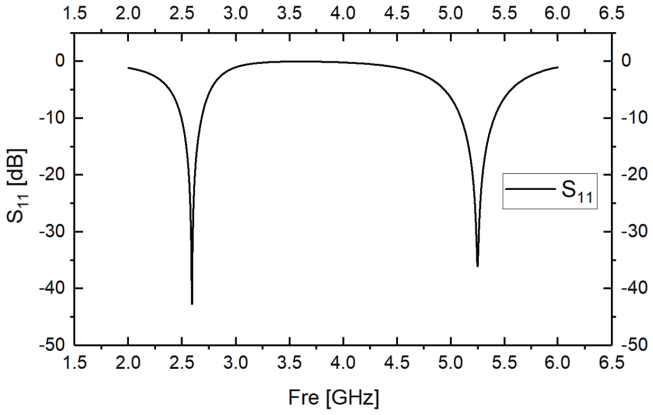

FIGURE 4. S_{11} of the miniaturized structure.

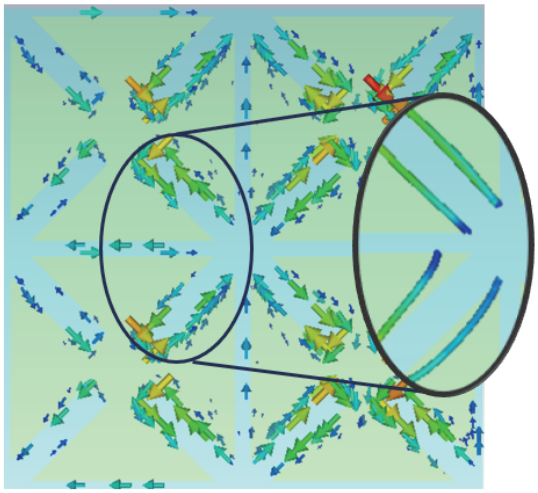

FIGURE 5. Current distribution of Malta cross structure.

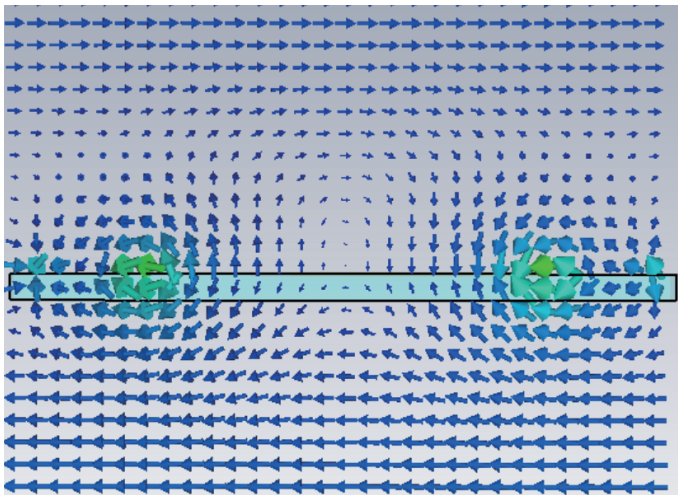

FIGURE 6. Electric field distribution of Malta cross structure.

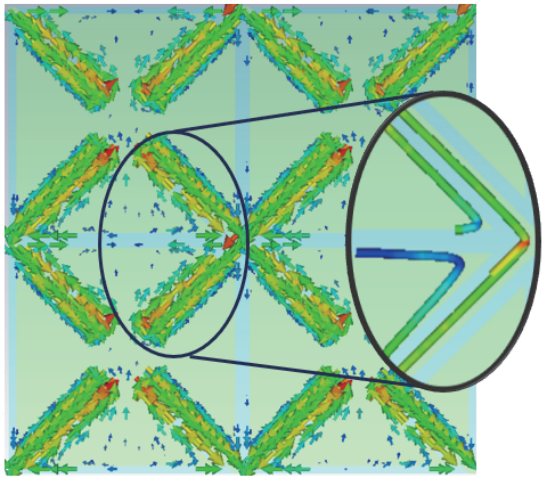

FIGURE 7. Current distribution of the miniaturized structure.

the resonance point at low frequency is not directly generated by the ordinary cross structure. Rather, the ordinary cross structure connects two units causing current to flow between the two units, which results in a doubling of the current path. Therefore, the frequency of the resonance point at low frequency is roughly half of the high frequency.

In addition, by analyzing the current paths of the unit and selecting a unit as volume element, the equivalent circuit diagram of a single unit can be obtained as shown in Figure 8. The entire unit can be seen as composed of two crosses, and the resonant circuit of the entire unit can be seen as composed of four separate parallel resonant circuits. In this circuit, C_{mp} represents the coupling capacitance between the regular cross arm and Malta cross arm. L_m represents the equivalent inductance of Malta cross arm. L_p represents the equivalent inductance of the regular cross arm, and L_{mp} represents the coupling inductance between the Malta cross arm and regular cross arm. In order to simplify the analysis process, the coupling capacitance between Malta cross arms and the coupling capacitance between the two elements are not considered here. By analyzing the equivalence, the unit size can be adjusted to achieve full transmission phases.

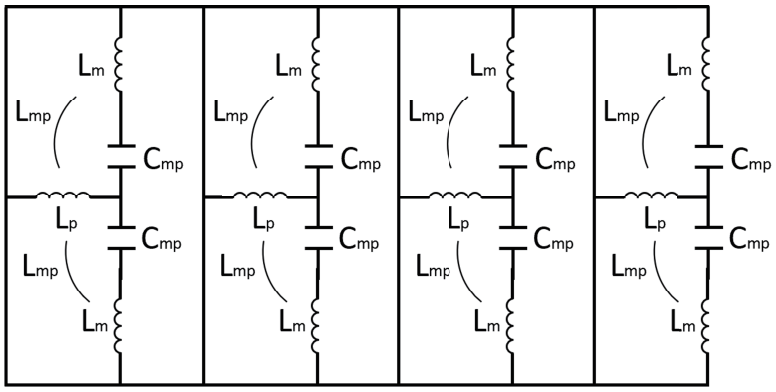

FIGURE 8. Equivalent circuit of a single unit.

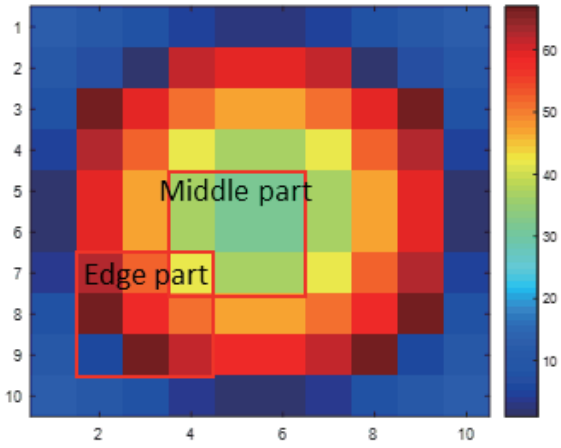

FIGURE 9. Malta cross array with 0°.

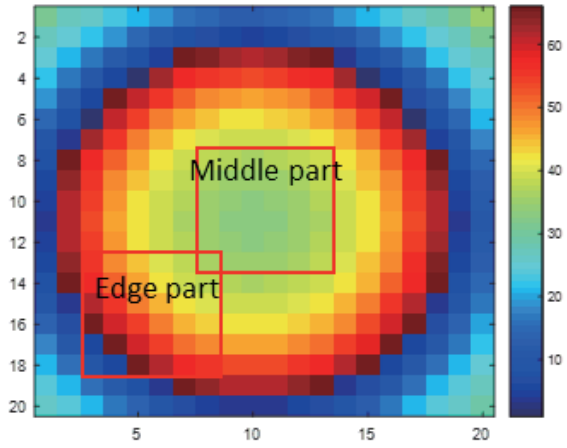

FIGURE 10. Miniaturized unit array with 0°.

4. ADVANTAGES OF MICROWAVE LENS IN MINIATURIZATION

In order to verify the capacity of miniaturized unit array, miniaturized unit array and Malta cross array are compared in this chapter. A square array of 500 mm × 500 mm is used in this study, with a focal length ratio of 0.8. The illumination is a 1 × 2 microstrip Yagi antenna array with a gain of 10 dBi. In order to prove the advantages of miniaturized units, a part of the entire array with the same relative phase is selected to compare.

The Malta cross array is shown in Figure 9. The size of each unit is 50 mm × 50 mm, and the scale of array is 10 × 10. The miniaturized unit array is shown in Figure 10. The size of each unit is 25 mm × 25 mm, and the scale of array is 20 × 20. The middle and edge parts of the entire array are selected for analysis. The scales of selected cells are 3×3 and 6×6, respectively. And the relative phase is 0°.

The return losses of different arrays with 0° are shown in Figure 11 and Figure 12. In the same region, the response frequency band of miniaturized unit array is larger than that of the Malta cross array. In the edge part with lager phase difference, the response frequency band of the miniaturized unit array is more than 2–3 GHz, while that of the Malta cross array is only 2.12–2.54 GHz. In addition, for different regions, the response of the miniaturized unit array varies much less than that of the Malta cross array.

The relative phase is one of the factors that affects the capacity of the array. The choice of relative phase will influence the capacity of array by affecting the value of the transmission phase and transmission amplitude. Thereby, the situation with different relative phases is analyzed. The relative phase of 20° is shown in Figure 13 and Figure 14.

The return losses of different arrays with 20° are shown in Figure 15 and Figure 16. S_{11} changes as the relative phase changes. However, the response frequency band of the miniaturized unit array is still larger than that of the Malta cross structure. It is shown that the miniaturized unit structure can reduce the influence between cells and expand response frequency band.

5. BEAM-SCANNING ALGORITHM BASED ON PHASE DISTRIBUTION OF POINT LIGHT SOURCE

In order to achieve the beam-scanning, an optimization algorithm to calculate the phase distribution of units is considered

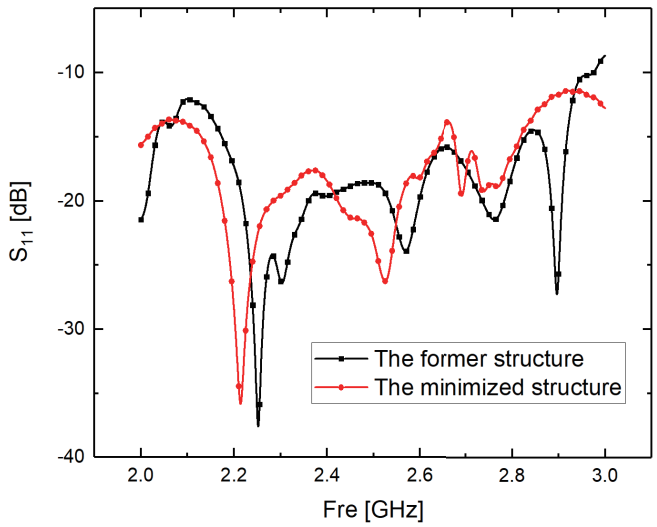

FIGURE 11. Return loss of middle part with 0°.

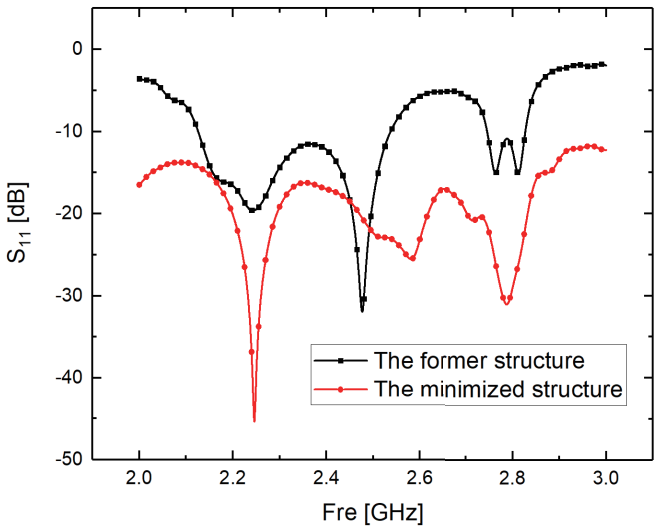

FIGURE 12. Return loss of edge part with 0°.

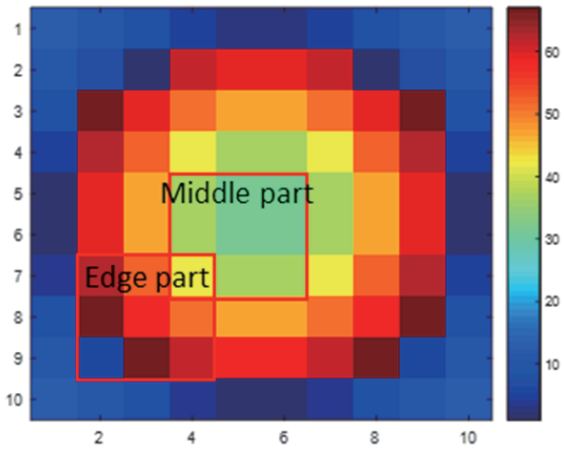

FIGURE 13. Malta cross array with 20°.

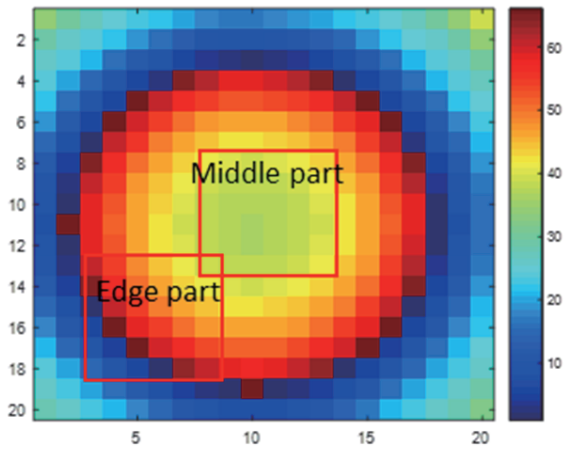

FIGURE 14. Miniaturized unit array with 20°.

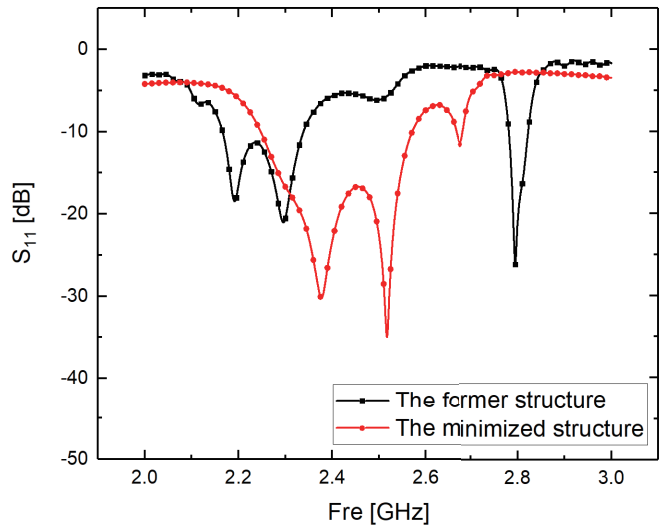

FIGURE 15. Return loss of middle part with 20°.

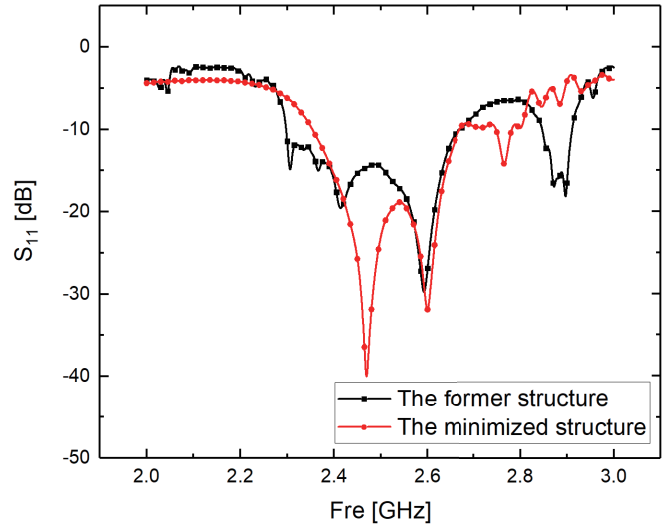

FIGURE 16. Return loss of edge part with 20°.

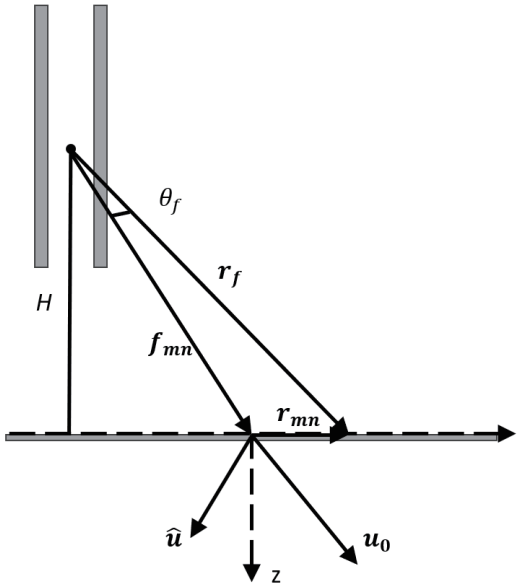

FIGURE 17. Schematic of mechanical scanning.

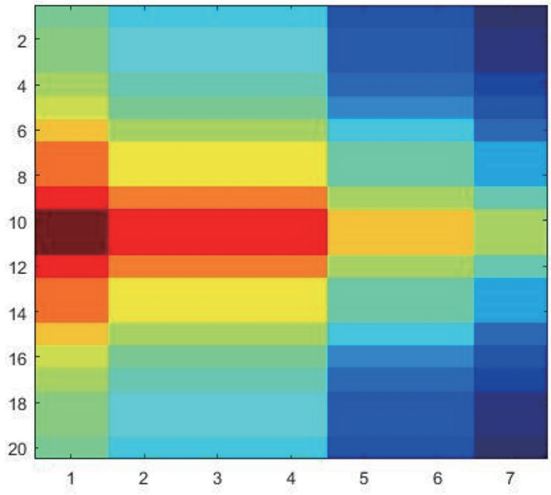

FIGURE 18. The first layer compensation.

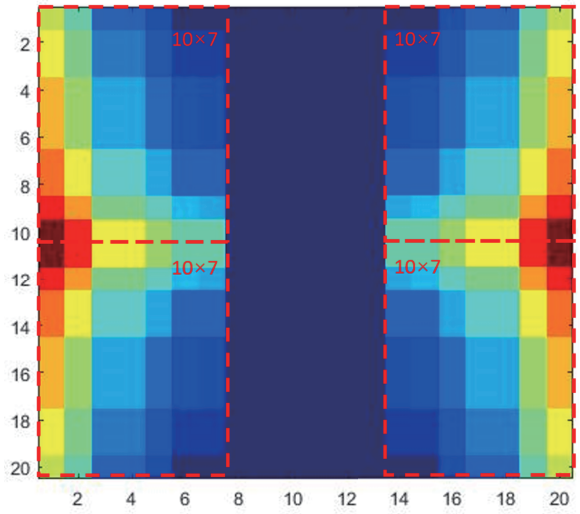

FIGURE 19. Region Division.

in this part. As shown in Figure 17, the illumination moves along the X-axis at a height of 400 mm above the array.

The field of the array, which is equal to the superposition of each unit field and the illumination field at each unit position, is determined by [18]

$$E(\theta,\varphi) = \sum_{m=1}^{M}\sum_{n=1}^{N}(\cos d(\theta))^{q_e}\cdot\left(\frac{\mathbf{r}_{mn}\cdot\mathbf{r}_f}{|\mathbf{r}_{mn}|\cdot|\mathbf{r}_f|}\right)^{q_f} \cdot e^{jk(\mathbf{r}_{mn}\hat{\mathbf{u}})}\cdot|T_{mn}|\cdot e^{j(\theta_{cmn}+\theta_{fmn})}/|\mathbf{r}_{mn}-\mathbf{r}_f| \quad (1)$$

where θ_{cmn} is the compensating phase, and θ_{fmn} is the phase of illumination.

The traditional particle swarm optimization (PSO) algorithm has the following problems: the local optimal solution is easy to get because of large search domain and huge number of particle swarm; the coupling between cells is difficult to predict out of the large differences between adjoining units; the optimized array has low robustness due to the lack of consideration for continuous variables.

To address these issues, an improved PSO algorithm is proposed. The core idea of this algorithm is to use quasi-regularly distributed particle positions instead of randomly distributed particle positions as shown in Figures 18. This not only reduces the search space but also makes the optimized phase distribution more uniform. The array is divided into three regions according to the illumination moving region and the electric field of illumination as shown in Figure 19. In different regions, quasi-ordered compensating phase is superimposed to achieve phase-shifting.

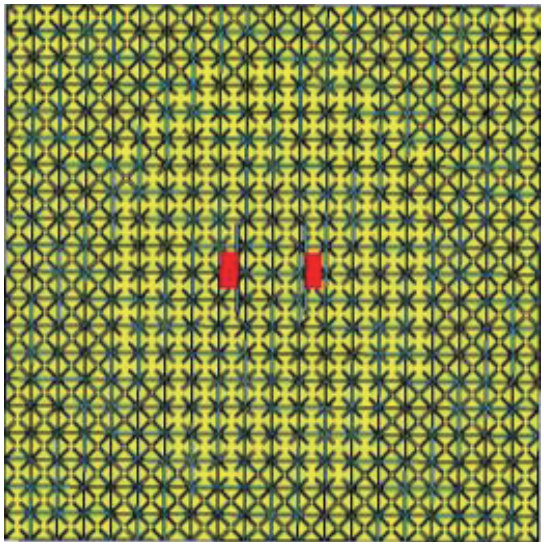

FIGURE 20. Array arrangement.

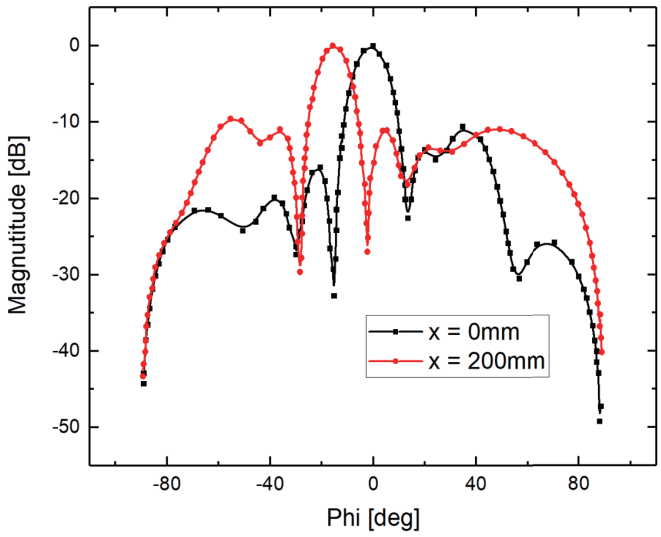

FIGURE 21. Matlab simulation result.

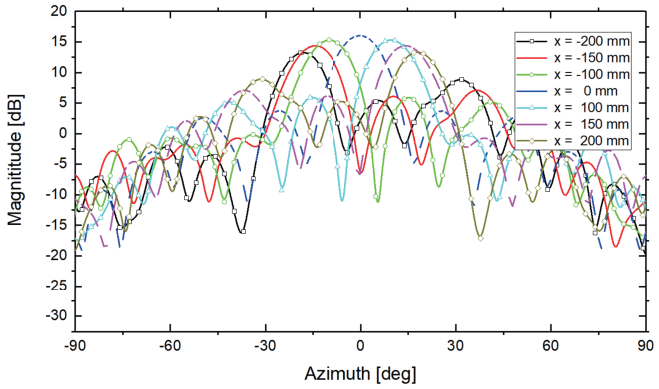

FIGURE 22. Gain of different displacements.

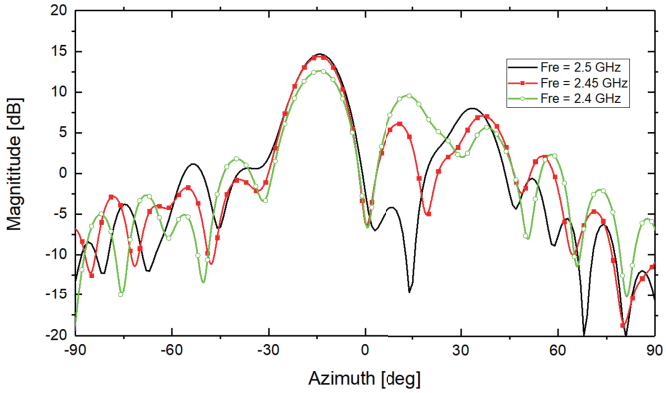

FIGURE 23. Gain of different frequencies at $x = 150$ mm.

TABLE 2. Main lobe angle of different illumination shift.

The shift of illumination (mm)	200	150	100	0	100	150	200
The angle of main lobe (°)	−18	−14	−10	0	10	14	18

6. EXPERIMENT VERIFICATION AND MEASUREMENT RESULTS

According to the above model, the positions of illumination, $x = 0$ mm and $x = 200$ mm, are optimized and the phase-shifting of the targets set to 0° and $> 15°$, respectively. Besides, the target side lobe is no more than -20 dB. The program is run on Matlab R2019a, and the optimized array is shown in Figure 20.

As shown in Figure 21, it can be seen that when $x = 0$ mm, the main beam angle is 0°, and when $x = 200$ mm, the main beam angle is 18°. The difference between the main lobe and side lobe is about -10 dB.

CST simulation results are shown in Figure 22. In order to verify the advantages of the optimized array, simulation analyses for different frequencies and different illumination positions are given. The results for different illumination positions are shown in Figure 22. It can be seen that as the illumination moves, the main beam scans from $-18°$ to 18°. The main beam gain changes no more than 2 dBi. The relationship between the shift of illumination and main lobe angle is shown in Table 2. The results at different frequencies are shown in Figure 23. It can be seen that the maximum gain does not vary much with frequency.

Table 3 presents a performance assessment of the lens antennas in comparison to other lens antennas. The proposed antenna combines the largest quantity of aperture efficiency within a compact structure.

After machining the lens system, near-field testing is carried out. The size of the lens is 500 mm × 500 mm × 76 mm, and

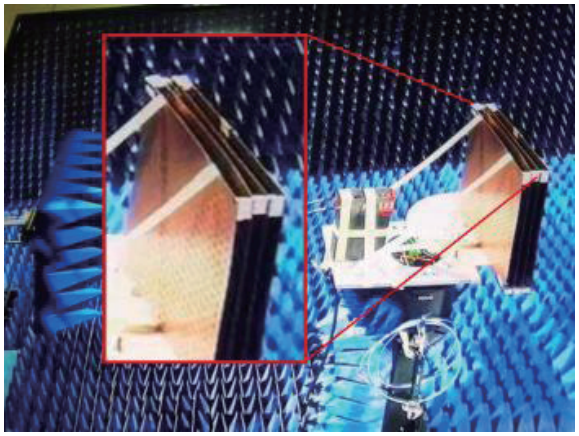

FIGURE 24. Test scene.

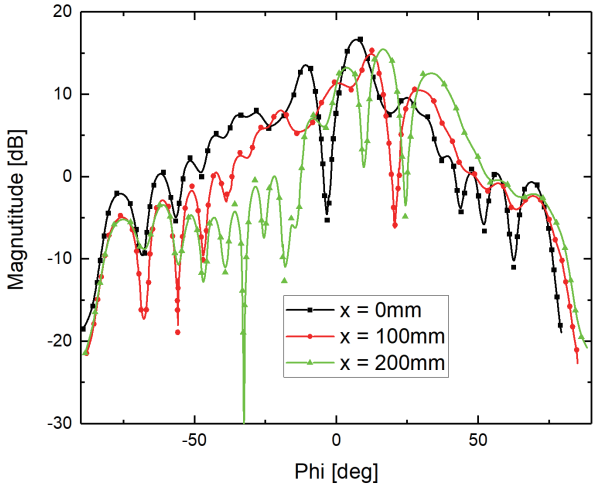

FIGURE 25. Near-field test results.

TABLE 3. Comparison of previous lens antennas.

Ref	f_0 (GHz)	Array size	Gain (dBi)	Phase-shifting (°)	e_a (%)
[19]	24	$3\lambda^2 \times \pi$	17.2	−36–36	-
[20]	30	$14.5\lambda \times 19.5\lambda$	27.3/24.5	0–50	15.1/7.9
[21]	28.5	$9.9\lambda \times 9.9\lambda$	25/19.5	−30–30	25/7.26
[22]	5.8	$10\lambda \times 10\lambda$	17.3/-	−37–37	4.5/-
This work	**2.45**	$\mathbf{4.09\lambda \times 4.09\lambda}$	**15.4/13.3**	**−18–18**	**16.5/10**

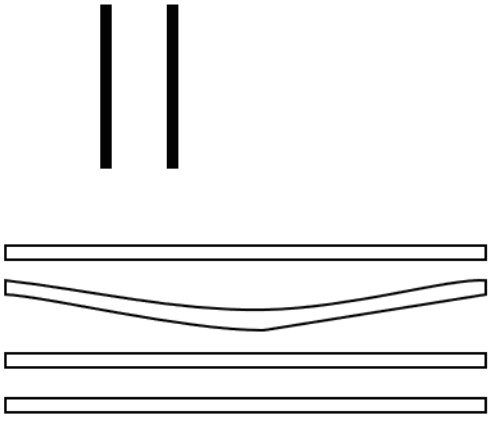

FIGURE 26. Curved lens model.

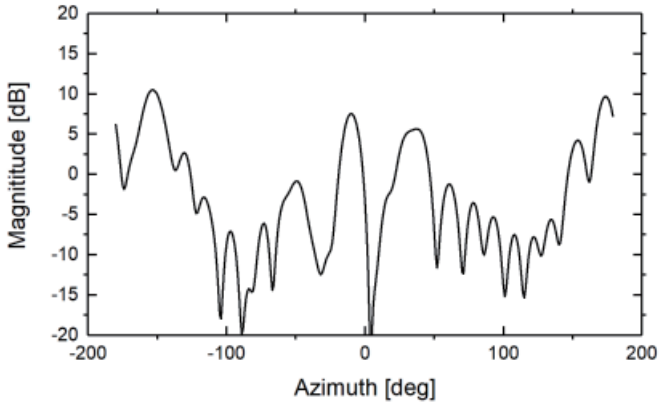

FIGURE 27. Gain of the curved lens.

the illumination is at a height of 330 mm above the lens. The lenses are supported by 25 mm plastic, and the Yagi antennas are supported by sponge. The test environment and test results are shown in Figure 24 and Figure 25. In addition to the machining error and environment error, it can be seen that the main lobe angle is basically consistent with that of simulation. However, because of the lens thickness and material, the plate bends, which makes the side lobe have a high level.

In order to verify the conjecture, the curved lens is analyzed. As shown in Figure 26, the second lens bending and the shift of the illumination by 100 mm are considered. The simulation results are shown in Figure 27. It can be seen that the main lobe angle is 10°, which is consistent with the results of the unbent lens. Due to the bending of the lens, the transmission phase and transmission amplitude of the unit change; the maximum gain decreases; and the side lobe increases.

7. CONCLUSION

In this manuscript, a miniaturized lens unit at 2.45 GHz is presented for WPT application. The idea of path reuse is proposed for miniaturization. The area of the miniatured structure with a size of 0.2×0.2 square wavelength is reduced to 16% compared to the half-wavelength structure. According to simulation

and measurement results, it can be seen that the miniaturized unit structure can reduce the influence between cells and expand response frequency band. In the end of this manuscript, through the quasi-ordered optimization idea, the beam scanning of $-18^\circ \sim 18^\circ$ is realized with the shift of the illumination in ± 200 mm.

REFERENCES

[1] Hoang, V. A. and Y. C. Lee, "Capacitive-wireless power transfer system for power supply of a wireless sensor system on a propulsion shaft," *Progress In Electromagnetics Research Letters*, Vol. 102, 9–18, 2022.

[2] Kurs, A., A. Karalis, R. Moffatt, J. D. Joannopoulos, P. Fisher, and M. Soljacic, "Wireless power transfer via strongly coupled magnetic resonances," *Science*, Vol. 317, No. 5834, 83–86, 2007.

[3] Cao, P., Y. Lu, C. Lu, and S. Wu, "Light-weight unmanned aerial vehicle wireless power transfer system based on hollow copper coated aluminum tubes," *Progress In Electromagnetics Research Letters*, Vol. 107, 49–57, 2022.

[4] Li, B., S. Liu, H.-L. Zhang, B.-J. Hu, D. Zhao, and Y. Huang, "Wireless power transfer based on microwaves and time reversal for indoor environments," *IEEE Access*, Vol. 7, 114 897–114 908, 2019.

[5] Summerer, L. and O. Purcell, "Concepts for wireless energy transmission via laser," *Europeans Space Agency (ESA) — Advanced Concepts Team*, 2009.

[6] Shinohara, N., "History and innovation of wireless power transfer via microwaves," *IEEE Journal of Microwaves*, Vol. 1, No. 1, 218–228, 2021.

[7] Zhu, X., K. Jin, Q. Hui, W. Gong, and D. Mao, "Long-range wireless microwave power transmission: A review of recent progress," *IEEE Journal of Emerging and Selected Topics in Power Electronics*, Vol. 9, No. 4, 4932–4946, 2020.

[8] Zheng, Q.-R., B.-C. Lin, and B.-H. Zhou, "Design of high gain lens antenna by using 100% transmitting metamaterials," *Progress In Electromagnetics Research C*, Vol. 86, 167–176, 2018.

[9] Veselago, V. G., "The electrodynamics of substances with simultaneously negative values of ε and μ," *Soviet Phys. Uspekhi*, Vol. 10, No. 4, 509–514, 1968.

[10] Cubukcu, E., K. Aydin, E. Ozbay, S. Foteinopoulou, and C. M. Soukoulis, "Negative refraction by photonic crystals," *Nature*, Vol. 423, 604–605, 2003.

[11] Antoniades, M. A. and G. V. Eleftheriades, "A broadband wilkinson balun using microstrip metamaterial lines," *IEEE Antennas and Wireless Propagation Letters*, Vol. 4, 209–212, 2005.

[12] Bonache, J., I. Gil, J. Garcia-Garcia, and F. Martin, "Novel microstrip bandpass filters based on complementary split-ring resonators," *IEEE Transactions on Microwave Theory and Techniques*, Vol. 54, No. 1, 265–271, 2006.

[13] Levine, R. C., "Transmission lines and wave propagation," *Proceedings of the IEEE*, Vol. 53, No. 10, 1682–1682, 1965.

[14] Li, T., D. Li, P. Qin, Y. Fan, Y. Gu, P. Zuo, W. E. I. Sha, and E. Li, "A novel miniaturized strong-coupled FSS structure with excellent angular stability," *IEEE Transactions on Electromagnetic Compatibility*, Vol. 63, No. 1, 38–45, 2020.

[15] Ma, L., L. Zhou, and C. Chen, "Broadband miniaturized bandpass frequency selective surfaces based on fractal transmissive metasurface elements," in *2018 IEEE 4th International Conference on Computer and Communications (ICCC)*, 336–340, IEEE, 2018.

[16] Sun, Y., Z. Li, W. Zhu, Z. Ji, and Q. Wang, "New steerable antenna with controllable metamaterial," in *2012 9th European Radar Conference*, 610–613, IEEE, 2012.

[17] Abdelrahman, A. H., F. Yang, A. Z. Elsherbeni, and P. Nayeri, *Analysis and Design of Transmitarray Antennas*, Morgan & Claypool Publishers, 2017.

[18] Eberhart, R. and J. Kennedy, "Particle swarm optimization," in *Proceedings of the IEEE International Conference on Neural Networks*, Vol. 4, 1942–1948, 1995.

[19] Vinnakota, S. S., R. Kumari, H. Meena, and B. Majumder, "Rectifier integrated multibeam luneburg lens employing artificial dielectric as a wireless power transfer medium at mm wave band," *IEEE Photonics Journal*, Vol. 13, No. 3, 1–14, 2021.

[20] Lima, E. B., S. A. Matos, J. R. Costa, C. A. Fernandes, and N. J. G. Fonseca, "Circular polarization wide-angle beam steering at Ka-band by in-plane translation of a plate lens antenna," *IEEE Transactions on Antennas and Propagation*, Vol. 63, No. 12, 5443–5455, 2015.

[21] Liu, G., M. R. D. Kodnoeih, K. T. Pham, E. M. Cruz, D. González-Ovejero, and R. Sauleau, "A millimeter-wave multibeam transparent transmitarray antenna at Ka-band," *IEEE Antennas and Wireless Propagation Letters*, Vol. 18, No. 4, 631–635, 2019.

[22] Han, J., L. Li, X. Ma, X. Gao, Y. Mu, G. Liao, Z. J. Luo, and T. J. Cui, "Adaptively smart wireless power transfer using 2-bit programmable metasurface," *IEEE Transactions on Industrial Electronics*, Vol. 69, No. 8, 8524–8534, 2021.